European Journal of Material Science
Vol.6, No.1, pp.1-20, December 2019
___Published by ECRTD-UK
Print ISSN: ISSN 2055-6551(Print), Online ISSN: ISSN 2055-656X(Online)

ENHANCING THE PERFORMANCE OF DYE SENSTIZIED SOLAR CELL BY INCOPORATING NANOPARTICLE

[1]Arthur Ekpekpo [2]Ukereti Gift Dafe

Department of Physics, Delta stateUniversity Abraka.

ABSTRACT*: This work was aimed at fabricating dye sensitized solar cell (DSSC) using chlorine e_6 as sensitizer and improving the light harvesting capacity of the device by incorporating AgNPs into the configuration using SILAR method. The optical characteristics of the sensitizer, AgNPs and photoanode of the device were determined using UV-Vis spectrophotometer and morphology of the mesoporous TiO_2 was determined using Scanning Electrode Microscope (SEM). The performance efficiency of the device was measured under Air Mass (AM) 1.5 at 100 mW/cm^2 solar simulation standard. The optical absorption characteristics of chlorine e_6 showed absorption peaks at 405, 503, 592 and 664 nm in the visible region. The maximum absorbance wavelengths (λ_{max}) of AgNPs were observed at 450, 455, 455, and 500 nm for 3, 6, 9 and 12 SILAR cycles respectively; these observed peaks correspond to a peculiar characteristic of the AgNPs surface plasmon resonance band and the red shift observed from 450 to 500 nm was attributed to coalescence of AgNPs at higher SILAR deposition cycles. The optical absorption spectrum of the photoanode was improved when AgNPs was introduced leading to increase in the absorption intensity; the intensity increases with the increase in SILAR cycles. The fabricated DSSC (0 SILAR cycle) relatively demonstrated low efficiency of 0.28% (short circuit current density [J_{sc}] = 1.07 mA, open circuit voltage [V_{oc}] = 0.46V, and fillfactor [FF] = 0.57) and was however enhanced with the incorporation of AgNPs. The cell with 6 SILAR cycles of AgNPs achieved photovoltaic efficiency of 0.43 % (J_{sc} = 1.39 mA, V_{oc} = 0.50 V, and FF = 0.62) at SILAR of 12 cycles, an efficiency of 0.54% was achieved for the DSSC. Thus, the incorporation of AgNPS into the photoanode effectively enhanced the light harvesting capacity and improved the overall efficiency of the DSSC using chlorine e_6 as photosensitiser.*

KEY WORD: Dye sensitized solar cell (DSSC), chlorine e6, Nanoparticle

INTRODUCTION

The increase in energy consumption as the world continuously depends on it for the sustainability has been the major cause of energy crisis our society faces today and the extensive use of fossil fuel is not only associated with environmental pollution, global warming and dimming but its reserve is also finite and non-renewable (Isahet *et al.,* 2016). This has called for the development and the utilisation of other clean and renewable alternative energy resources; scientists and engineers have successfully made use of a variety of green energy sources like tidal, biomass, geothermal, wind, hydroelectric and solar energy (Kukreja, 2015).

A lot of resources and efforts are currently being channelled towards the development of these renewable energy technologies in order to address the impending challenges and so also to take control of most of the energy production; consequently, this effort has given rise to the continued decline in prices for renewable energy technologies which can now compete with fossil fuels. Though at present, most of the existing renewable energy technologies largely depend on weather conditions and integrating them into the grid system is quite challenging (Blaabjerg and Ionel, 2015).Among the existing clean and renewable energy resources, solar energy is one of the most promising of which other sources are limited in their applications due to geographical conditioning (Smestad, 2002). Photovoltaic (PV) technology is considered as the leader in renewable power generation and a cost-competitive source of new power generation in many emerging markets across the world (REN21, 2017). On-going research and development efforts in the sector have shown that much still need to be done in order to enable large scale deployments of this technology to ensure economic feasibility; many have recognised large devices and power plants as the key players of the economy of scale, including lower cost of energy (Jolayemi, 2016).

Photovoltaic (PV) technology has been a focal point of research in energy sector, the development of this technology has witnessed different innovative phases right from the first generation whose technology is based on crystalline silicon (c-Si) and made up of the major current commercial production. On the other hand, the second generation is focused on the thin film technology which covers the range of thin films materials such as cadmium telluride (CdTe), amorphous-silicon (a-Si) and copper (gallium) indium selenide/sulphide (CIGS) (Jolayemi, 2016). The latest innovation involves the multi-junction concepts and emerging fields of optical metamaterials of which Dye-Sensitised Solar Cells (DSSCs) is a key player.

DSSCs was first developed by O'Regan and Gratzel (1991), the principle employed organic dyes adsorbed nanocrystalline titanium dioxide (TiO_2) films to absorb light from sun and generate electricity. From the inception of this technology, many remarkable landmarks have been recorded by developing solid electrolytes, introducing of perovskite solar technology, commercialising the device and raising the efficiency of the device up to the present 22.1% of perovskite solar cells, among others.

On the other hand, surface modification of photoanode is considered as an important way of enhancing the efficiencies of the device and one of the several means of achieving this is the incorporation of plasmonic nanomaterials (Isah *et al.*, 2016). The introduction of these materials into the configuration of the solar cells has been reported to have significantly improved the device efficiencies owing to their localised surface plasmon (LSP) effect (Jolayemi, 2016; Isah *et al.*, 2016; Xu *et al.*, 2013). The LSP effect is one of the most captivating features of these nanomaterials with the ability to strongly absorb and scatter radiation in the visible region (Jolayemi, 2016; Jing *et al.*, 2013).

MATERIALS AND METHOD

Materials

The materials used for this research work are divided into consumables and equipment. The consumables used for the synthesis of silver nanoparticles (AgNPs) include:

i. Silver nitrate ($AgNO_3$) (BDH)
ii. Stannous chloride ($SnCl_2.2H_2O$) (BDH)
iii. Ammonium solution (NH_3OH) (*ca.* 33 %wt NH), (Grifflin and George)
iv. hydrochloric acid (HCl) (36%) (Loba Chemie)
v. Distilled water

While the consumables used for the fabrication of the DSSCs include:

i. Sensitiser (chlorin e_6, dye based on a chlorophyll derivative extracted from spinach acquired from Namiroch Nig. LTD).
ii. Conductive glass substrate (FTO: TCO30-8 glass, 8Ω/sq, 3mm thick) (Solaronix)
iii. Nanostructured TiO_2 paste (Ti-Nanoxide T300/SP), (Solaronix)
iv. Platinum (Pt) counter-electrode (Platisol T/SP), (Solaronix)
v. Sealing polymer sheet (SX1170-25PF), (Solaronix)
vi. Electrolyte (Iodolyte HI-30) (Solaronix)

The equipment and other materials used for the synthesis and fabrication include:
Weighing balance, Beakers, Magnetic stirrer, Soda lime glass substrates, Petri dishes, Profilometer, screen printer, solar simulator and UV/Visible spectrophotometer (Axiom Medicals UV752).

METHODS

Preparation of Photoanode

The layer of mesoporous TiO_2, dye and plasmonic silver nanoparticles on conducting glass substrate (Fluorine doped tin oxide (FTO) glass) forms the photoanode of the device. The preparation of the photoanode started with the cleaning and degreasing of 2.5 x 2.5 cm^2 FTO glass with soap (Sodium Lauryl), rinsed with distilled water, ethanol and allowed to dry naturally.

Preparation of Plasmonic AgNPs

Silver nanoparticles (AgNPs) were prepared by successive ionic layer adsorption and reaction (SILAR) method using diammine silver complex and stannous chloride as starting materials i.e. cationic and anionic precursor. The cationic precursor for the SILAR method was diammine silver complex $\left([Ag(NH_3)_2]^+_{(aq)}\right)$ solution. This solution was prepared using 0.35g of $AgNO_3$ in 200ml of distilled water, to this, ammonia solution (NH_3OH) was added dropwise until colourless solution was observed and 0.01M concentration was obtained. The anionic (reducing agent) solution was prepared by adding 2 ml of concentrated HCl to 2g of stannous chloride ($SnCl_2.2H_2O$) in 640 ml of distilled water to obtain 0.2M concentration.

Sensitisation of Photo-anode

The prepared layer of AgNPs and TiO_2 on FTO glass substrates were soaked the sensitizing dye containing chlorin e_6 for about 18 hours for photoanode impregnation after which the photoanodes were rinsed with ethanol in order to remove excess dye particles that were not properly adsorbed.

Fabrication of DSSCs

A sandwich-type DSSCs were fabricated by assembling the dye impregnated photoelectrodes and counter-electrodes in an overlapping manner so as to establish electrical connection between the cells and the photovoltaic measurement equipment. The assembling was achieved by using hot-melt sealing gasket of surlyn based polymer sheet (SX1170-25PF, Solaronix) and sealed on a heating stage leaving a pinhole for the electrolyte injection for a few seconds. And finally, the iodine based liquid electrolyte (iodolyte) was injected using micropipette before sealing with hot-melt sealing gasket. After the fabrication process of the DSSCs the various thin films were characterised using UV spectrophotometer.

Morphological Characterization of Thin Films

A Scanning Electron Microscope (SEM) is a type of electron microscope that images a sample by scanning it with a high-energy beam of electrons in a raster scan pattern. The electrons interact with the atoms that make up the sample producing signals that contain information about the sample's surface topography, composition, and other properties such as electrical conductivity. The types of signals produced by an SEM include secondary electrons, back-scattered electrons (BSE), characteristic X-rays, light (cathodoluminescence), specimen current and transmitted electrons. Secondary electron detectors are common in all SEMs, but it is rare that a single machine would have detectors for all possible signals. The signals result from interactions of the electron beam with atoms at or near the surface of the sample.

Efficiency Measurement of DSSC

The current-voltage characteristics of each cell were recorded with a solar simulator, Keithley 2400-SCS source meter using a 300 W xenon light source (Newport Oriel 91160-1000) equipped with AM1.5 filter, which was focused to give a light intensity 100 mW/cm^2, on the surface of dye-sensitised TiO_2 photoanodes. In order to reduce scattered light from the edge of the TiO_2 photoanodes, a light shading mask was used to cover the DSSC to fix an active area of 0.36 cm^2. The current output of each cell was recorded by linearly varying the potential from -0.1 to 0.8 V in a 4-wire configuration.The photovoltaic parameters: maximum power output (P_{max}), fill factor (FF), and conversion efficiency (η) of the devices were evaluated according to the following formula relationship based on J-V characteristic curves in the following equations:

$$P_{\max} = V_{\max} \times J_{\max}$$

$$Fillfactor\left(FF\right) = \frac{P_{\max}}{V_{oc} J_{sc}} = \frac{V_{\max} J_{\max}}{V_{oc} J_{sc}}$$

$$Efficiency(\eta) = \frac{FF \times V_{oc} \times J_{sc}}{P_{in}} \times 100$$

RESULTS AND DISCUSSION

Optical Absorption Characteristics of Chlorine e_6 Based Sensitiser

The absorption characteristics of the dye sensitizer describes the optical transition probability between the ground state, the excited state and the solar energy range that can be absorbed by the dye (Isah *et al.*, 2016). The chlorine macrocycle forms the core structure in natural chlorophylls, Chlorine e_6 has been identified with three terminal carboxyl groups, with this feature, electrons can be efficiently injected from the chlorine macrocycle to TiO_2, hence, chlorine-based chlorophylls can be said to be suitable for solar cell applications (Wang *et al.*, 2013; Wang and Kitao, 2012). The optical absorption characteristics of chlorine e_6 in the near UV and visible region is shown in Figure 1. The absorption spectra of the Chlorine e_6 in the visible region show a maximum at 405, 503, 592 and 664 nm.

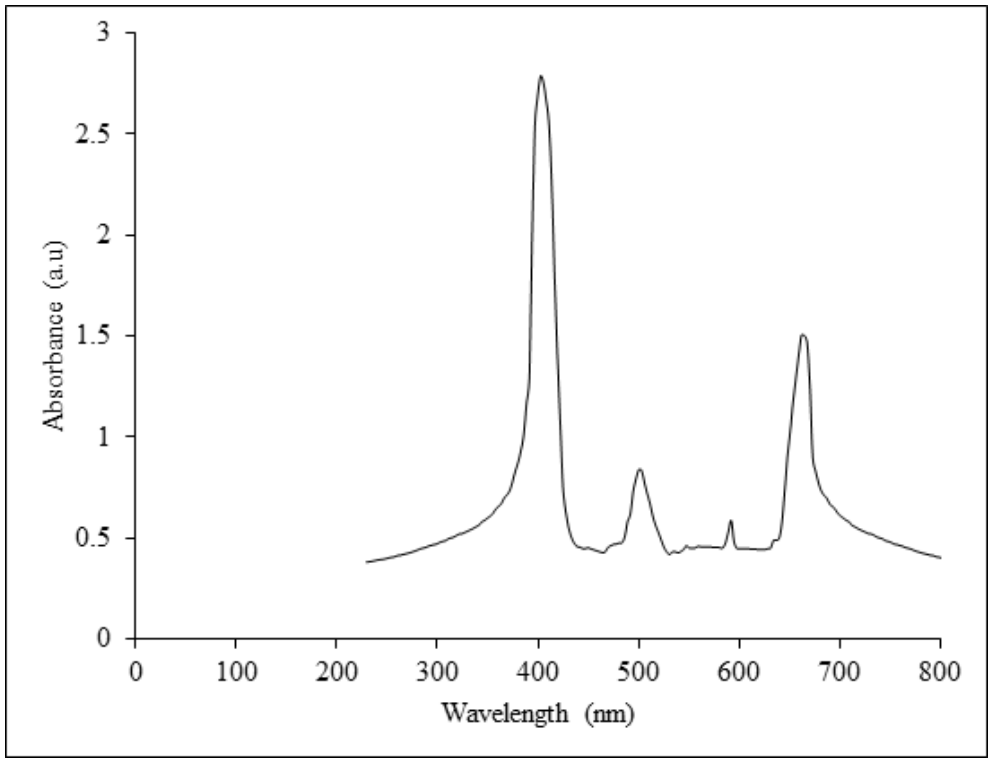

Figure 1: Absorption spectra of the Chlorine e6 based dye

This result indicates that Chlorine e_6 has a potential to function as an efficient sensitizer for wide bandgap semiconductors like TiO_2 using visible light for sensitisation in order to achieve high photovoltaic efficiency for a solar cell (Amao and Komori, 2004; Lightbourne *et al.*, 2015).

Optical Characteristics of Ag NPs

The optical properties of the silver nanoparticle are owing to the interaction between incoming light and free conduction electrons. When the wavelength of the incident light matches with the oscillating frequency of the conduction electron, a surface plasmon resonance occurs, this gives rise to the absorption band in the visible region. This surface plasmon resonance peak depends on the particle size, shape, surface charge, separation between the particle and the nature of the environment. The surface structure of the nanoparticles determines the charge of the nanoparticles (Thamilselvi and Radha, 2017).

Silver nanoparticles absorb and scatter light with extraordinary efficiency. Their strong interaction with light occurs because the conduction electrons on the metal surface undergo a collective oscillation when they are excited by light at specific wavelengths (Nanocomposix, 2017). This oscillation is known as a surface plasmon resonance (SPR), and it causes the absorption and scattering intensities of silver nanoparticles to be much higher than identically sized non-plasmonic nanoparticles. Silver nanoparticle absorption and scattering properties can be tuned by controlling the particle size, shape, and the local refractive index near the particle surface (Nanocomposix, 2017). In general, the optical properties of the plasmonic materials like silver nanoparticles have a tremendous influence on the scattering and surface plasmon resonance effects of the materials.

The UV-Vis absorption spectra of as-synthesised silver nanoparticles on glass substrate for 3, 6, 9 and 12 SILAR cycles are shown in Figure 2 (a-d).

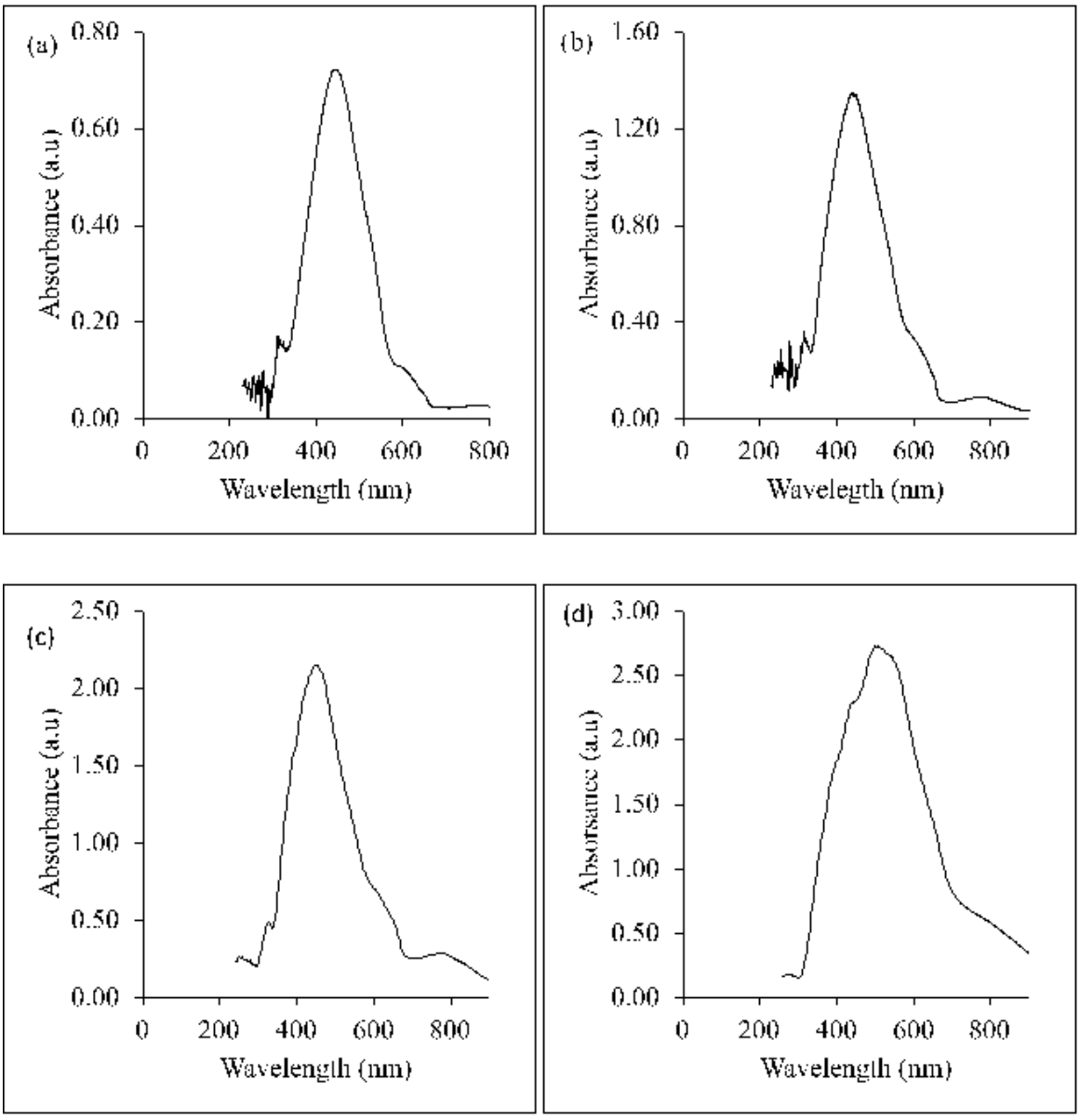

Figure 2(a-d): The UV-Vis absorption spectra of SILAR synthesised silver nanoparticles on glass substrate at (a) 3, (b) 6, (c) 9 and (d) 12 cycles

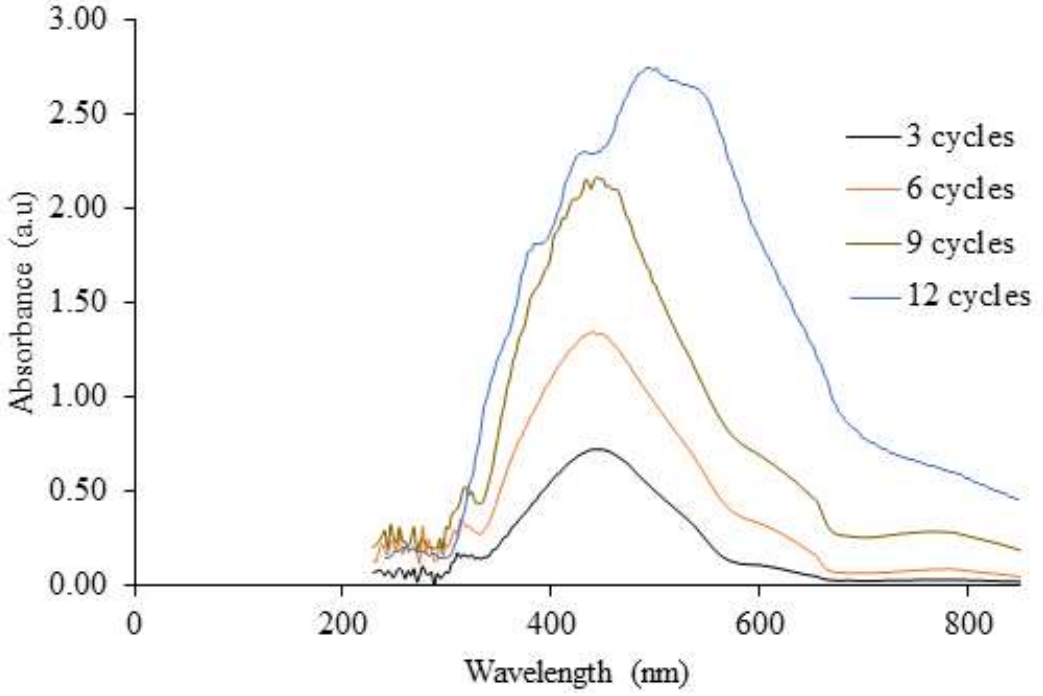

Figure 3: Optical absorption spectra of Ag NPs on glass substrate at different SILAR cycles

It is clear from the absorption spectra that the maximum absorbance wavelengths (λ_{max}) are 450, 455, 455, and 500 nm for 3, 6, 9 and 12 SILAR cycles respectively. There is a red shift from 450 to 500 nm by increasing the SILAR cycles from 3 to 12 cycles. This red shifting may be due to the increasing in size of the nanoparticles by increasing the SILAR cycles as a result of coalescence of Ag nanoparticles at higher SILAR deposition cycles (Isah *et al.*, 2016; Gharibshahi *et al.*, 2017; Zong *et al.*, 2014).

On the other hand, the main absorption peaks observed at around 450, 455, 455, and 500 nm for 3, 6, 9 and 12 SILAR cycles are corresponding to a peculiar characteristic of the silver nanoparticles surface plasmon resonance band (Thiwawong *et al.*, 2013; Zong *et al.*, 2014). It is found that the main absorption peaks were slightly red shifted when the SILAR cycle increased. This result agrees well with the Mie theory for the surface plasmon peak of nanoparticles in UV-visible absorption spectra; according to the Mie theory, silver nanoparticles of diameters ranging from 1 to 10nm have the plasmon peak width increasing linearly with the reciprocal of the particle diameter (Thiwawong *et al.*, 2013; Mafune *et al.*, 2000; Petit *et al.*, 1993).

Optical Characteristics of Photoanode

The optical spectra of the photoanode containing mesoporous TiO_2 and plasmonic silver nanoparticles with different SILAR cycles are presented in Figure 4 (a and b).

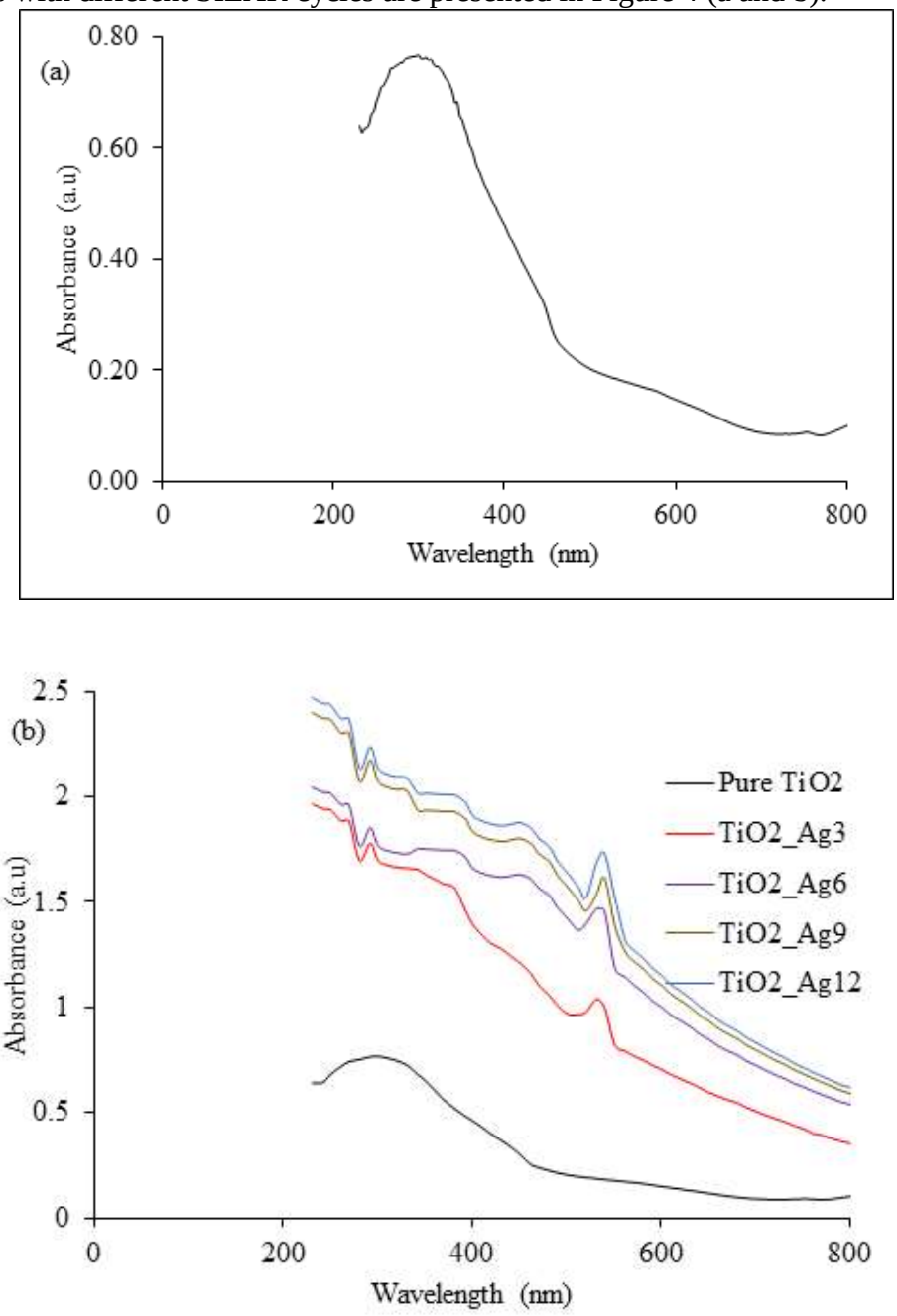

Figure 4: Absorption spectra of (a) pure mesoporous TiO_2 (b) AgNPs SILAR incorporated mesoporous TiO_2

The absorption spectrum (as illustrated in Figure 4a) of the mesoporous TiO_2 indicates low absorbance at the visible and near infrared regions but shows a strong absorption at the UV region with a broad peak around 300 nm. Figure4b shows the absorption spectra of the photoanode (m-TiO_2) containing AgNPs with 3, 6, 9 and 12 SILAR cycles; with the presence of the AgNPs, the spectra indicate improvement in the light absorption capability of the photoanode across the entire UV-visible spectrum leading to increase in the absorption intensity. The intensity increases as the SILAR cycles increase from 3 to 12. All the photoanode exhibit sharp absorption peak at 530 nm in the visible region. The absorption improvement can be attributed to localized surface plasmons (LSP) effect of the AgNPs (Isah *et al.*, 2016)

Current-Voltage (J-V) Characteristics of the Device

The current density-voltage (J-V) measurement of solar cells evaluates performance efficiency of the cell. The J-V curve characteristics of the DSSCs exploring Chlorine e_6 dye extract as a sensitizer were determined to study the effect of plasmonic Ag nanoparticles (Ag NPs) on the photovoltaic performance of the dye-sensitised solar cells (DSSCs) under AM 1.5 solar irradiation conditions (100 mW/cm^2). Evaluation of the photovoltaic performance was done through the analysis of open-circuit voltage (V_{oc}), short-circuit current (I_{sc}), fill factor (FF), and energy conversion efficiency (η) as shown in Figure 5.

The efficiency was calculated using the relation;

$$\text{Efficiency}(\eta) = \frac{FF \times V_{oc} J_{sc}}{P_{in}} \times 100\%$$

$$\text{Fill factor}(\text{FF}) = \frac{V_{\max} \times J_{\max}}{V_{oc} J_{sc}} = \frac{P_{\max}}{V_{oc} J_{sc}}$$

where P_{in} = 100 mW/cm^2, V_{max} and J_{max} are the voltage and the current density at the maximum power output respectively and P_{max} is the maximum power output.

Figures 5 and 6 show the J-V characteristic curves of the incorporated plasmonic AgNPs solar cells with different SILAR cycles, the cells are depicted as AgCell0, AgCell3, AgCell6, AgCell9 and AgCell12 for 0, 3, 6, 9 and 12 SILAR cycles respectively. The values for the photovoltaic parameters of the cells are given in Table 1. The main points on the figures are J_{sc} (the maximum current at zero voltage), Voc (the maximum voltage at zero current), J_{max} (current density at the maximum power point) and V_{max} (voltage at the maximum power point). The product of J_{max} and V_{max} gives maximum power (P_{max}) output generated by the device while the fill factor is the ratio of the P_{max} to the product of J_{sc} and Voc which defines the squareness of the curve. The value of fill factor (FF) of a good cell tends towards unity (Duran *et al.*, 2012).

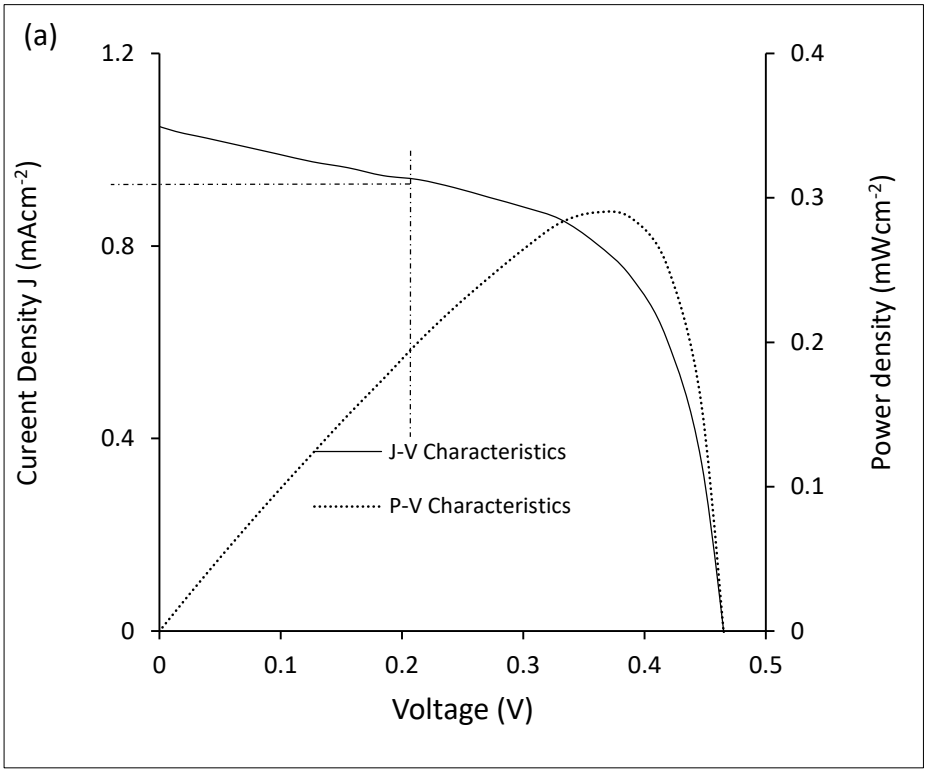
(a)
1.2
0.8
0.4
0
0.4
0.3
0.2
0.1
0
0
0.1
0.2
0.3
0.4
0.5
Cureent Density J (mAcm-2)
Power density (mWcm-2)
Voltage (V)
J-V Characteristics
P-V Characteristics

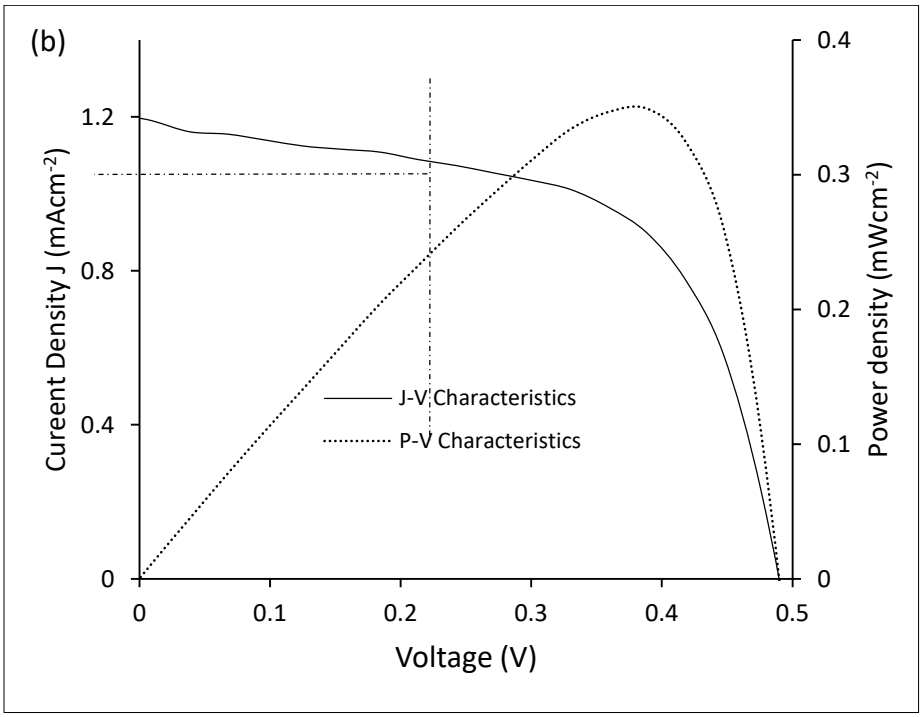
(b)
1.2
0.8
0.4
0
0.4
0.3
0.2
0.1
0
0
0.1
0.2
0.3
0.4
0.5
Current Density J (mAcm-2)
Power density (mWcm-2)
Voltage (V)
J-V Characteristics
P-V Characteristics

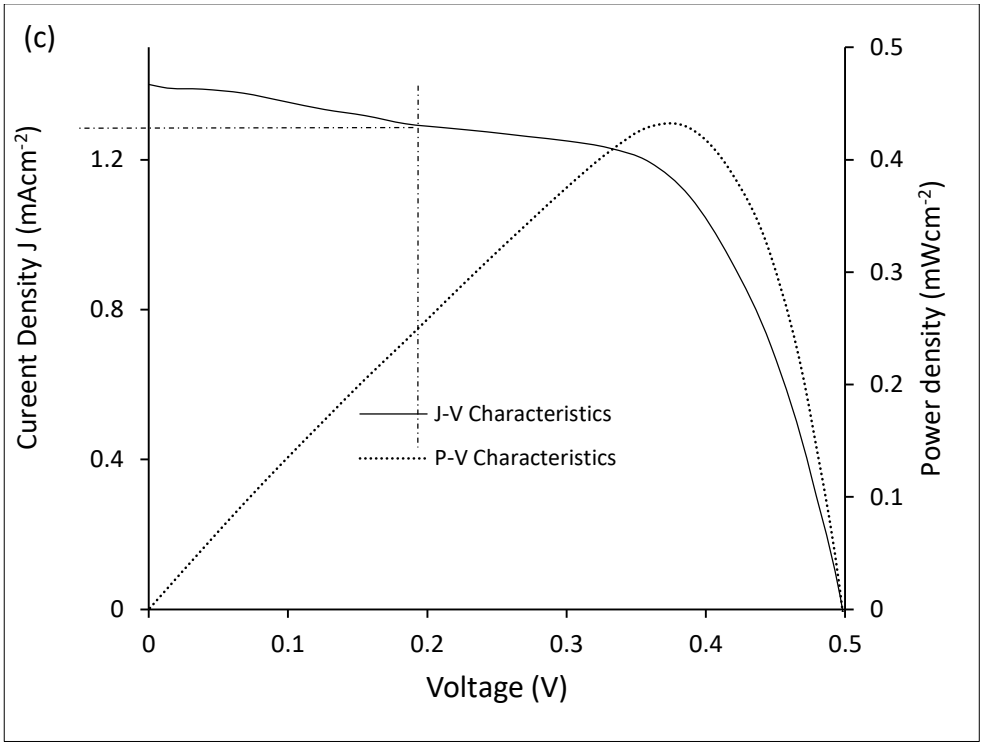
(c)
Cureent Density J (mAcm-2)
Power density (mWcm-2)
Voltage (V)
J-V Characteristics
P-V Characteristics
0
0.4
0.8
1.2
0.1
0.2
0.3
0.5

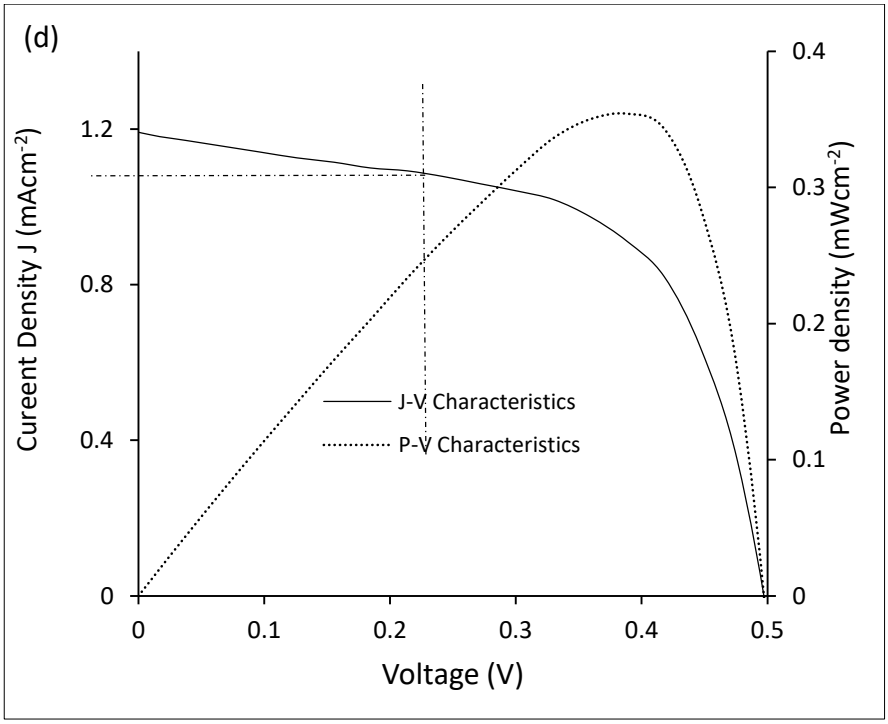
(d)
Cureent Density J (mAcm-2)
Power density (mWcm-2)
Voltage (V)
J-V Characteristics
P-V Characteristics
0
0.4
0.8
1.2
0.1
0.2
0.3
0.5

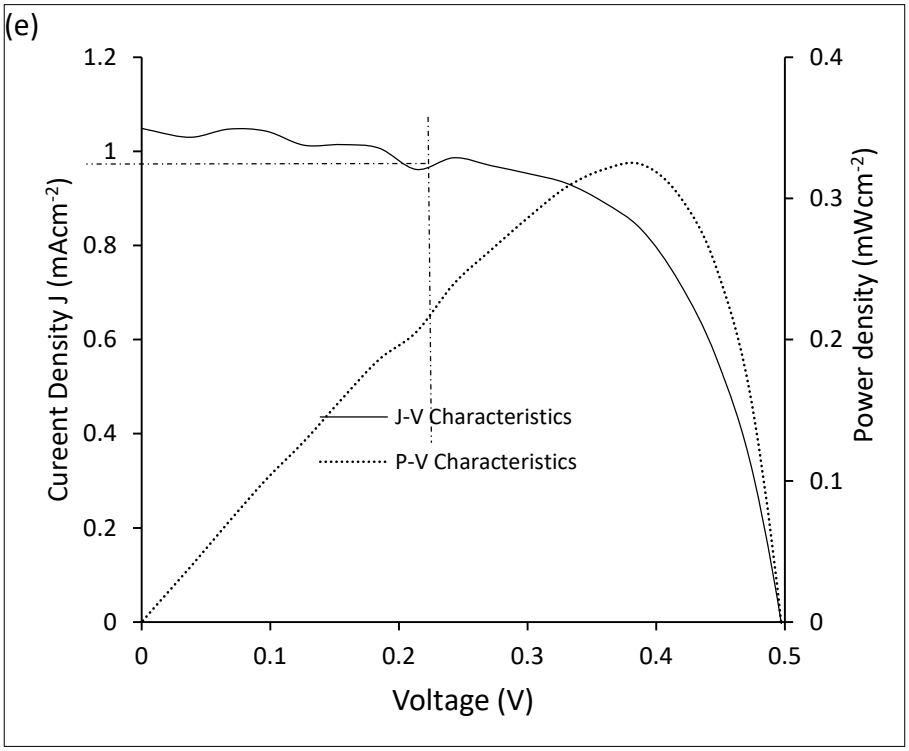

Figure 5: J-V and P-V characteristics of (a) Agcell0 (b) AgCell3 (c) AgCell6 (d) AgCell9 and (e) AgCell12

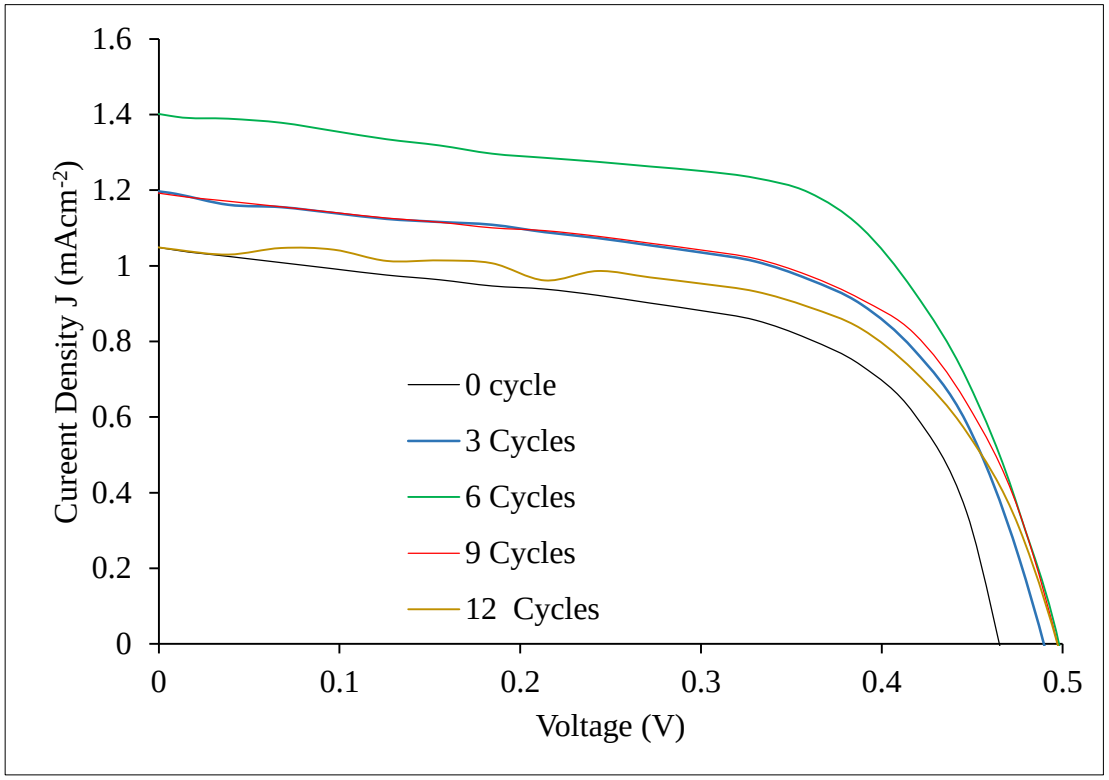

Figure 6: Comparison of the cells performance efficiencies at different SILAR cycles

Table 1: Photovoltaic parameters of DSSCs with different Ag SILAR cycles

S.No	SILAR Cycles	J_{sc} (mA)	V_{oc} (V)	FF	η (%)	% increase in η
1	0	1.07	0.46	0.57	0.28	0.00
2	3	1.2	0.49	0.58	0.34	21.23
3	6	1.39	0.50	0.62	0.43	54.27
4	9	1.20	0.50	0.60	0.36	27.78
5	12	1.16	0.50	0.57	0.33	18.06

Generally, the cells demonstrate good efficiency by employing chlorine e_6 as photosensitizer when compared to other similar solar cells sensitized with natural dyes as reported in the literature but they are mostly poorer than their synthetic counterparts (Blaabjerg and Ionel, 2015). The good efficiency results could be attributed to the terminal carboxyl groups which establish an electronic coupling with the 3d conduction band orbital manifold of Ti, the carboxyl groups which are essential for anchoring the dye molecules on the surface of TiO_2 (Amao and Komori, 2004). In addition, the performance could also be as a result of absorption capability of chlorine e6 in the visible region which would increase the light harvesting efficiency of the photoanode.

The effects of the Ag NPs on the performance of the DSSCs, indicate significant modifications to the photovoltaic parameters (J_{sc}, V_{oc}, and FF) of the cells as the SILAR cycles were varied and in return, made changes to the performance efficiency of the cell. AgCell0 exhibits 0.28 % efficiency (J_{sc} = 1.07 mA, V_{oc} = 0.46V, and FF= 0.57) which is taken as the reference cell and Ag NPs was incorporated into the cell configuration with 3 SILAR cycles the efficiency increased to 0.34 % (J_{sc} = 1.20 mA, V_{oc} = 0.49 V, and FF= 0.58), increasing the cycles to 6 as well increased the efficiency further to 0.43 % (J_{sc} = 1.39 mA, V_{oc} = 0.50 V, and FF= 0.62), the cycles were then increased to 9 which as a result dropped the efficiency to 0.36 % (J_{sc} = 1.20 mA, V_{oc} = 0.50 V, and FF= 0.60) before finally increased to 12 cycles with 0.33 % (J_{sc} = 1.16 mA, V_{oc} = 0.50 V, and FF= 0.57).

The effects of Ag NPs on the cell efficiency can be explained by the quantum and surface phenomenon associated with the properties of this material. The incorporation of Ag NPs into DSSCs modifies the interaction of the incoming light and the surface of the TiO_2 through their strong light absorption (as observed in the UV-Visible absorption spectra) and scattering activity as a result of Localised Surface Plasmon Resonance (LSPR) which stem from a collective oscillation of the surface electrons that occurs when light interacts with a particle at its resonant frequency (Jolayemi, 2016; Isah *et al.*, 2016; Amiri, Nouhi and Azizian-Kalandaragh, 2015; Jing *et al.*, 2013).

Considering these effect, the efficiency experiences different level of enhancements with the different cycles, about 21 % improvement was achieved when 3 SILAR cycles of Ag NPs was introduced over the reference cell, AgCell0. AgCell6 with photovoltaic efficiency of 0.43 % exhibits the highest improvement and came out best performing cells, this is about 54 % improvement over AgCell0. At the same time, there are increases in their corresponding generated photocurrent densities (J_{sc}) indicating an improvement in electron transport efficiency in the $nTiO_2$/dye/electrolyte interface as illustrated in Figure 7. The relationship between the obtained power conversion efficiency and the SILAR cycle is given in Figure 8.

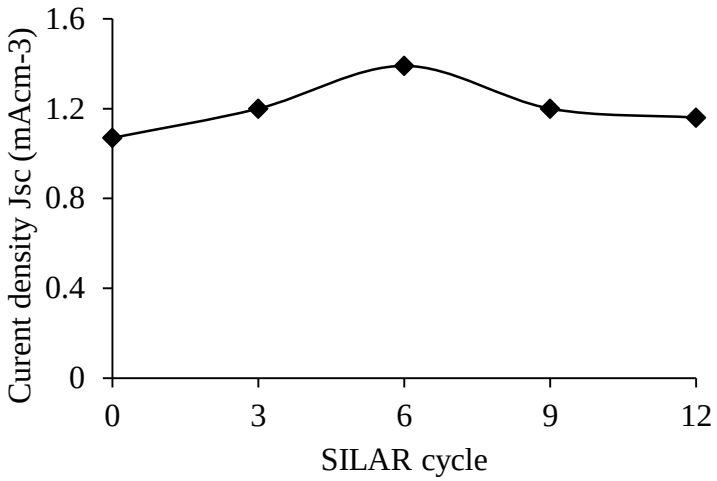

Figure 7: Short circuit current density (J_{sc}) and power conversion efficiency against different Ag SILAR cycles

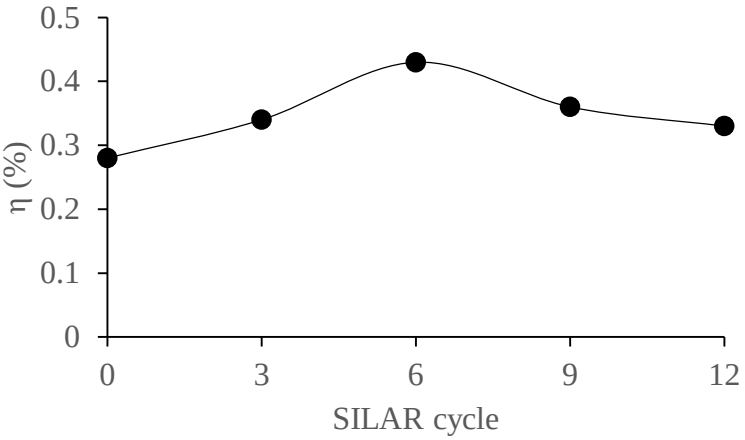

Figure 8: Power conversion efficiency versus SILAR cycle

In contrast, the continuous drop in power conversion efficiency as observed in Figure 4.6 when the cycles were further increased from 6 to 9 and then 12 may originate from recombination probability leading to the decrease in photocurrent density. Isah *et al.* (2016), incorporated Ag NPs using SILAR method into DSSCs but different cell architecture, observed that as SILAR cycles increases, then the Ag nanoparticles aggregate to form larger particles and creates defects at the

surface of the active layer of the cell which are potential recombination centres capable of trapping generated carriers; the surface recombination has a potential to negatively affect the carrier lifetime and as a result reduce the efficiency of the solar cells (Isah *et al.*, 2016). The recombination reaction could generate an internal short-circuit within the photoanode layer and result to poor J_{sc} and a low efficiency as observed in AgCell9 and AgCell12 contrary to expected improvement. Meanwhile, scattering effect of the NPs may be the major contributor to the efficiency decline, but the surface plasmon effects still dominates owing to the relatively small size of the nanoparticles (Xu *et al.*, 2014; Jolayemi, 2016).

CONCLUSION

This research work was aimed at fabricating DSSCs using chlorine e_6 as sensitizer and improving the light harvesting capacity of the device by incorporating AgNPs into the configuration. Hence, this study has successfully fabricated DSSCs with chlorine e_6 as sensitizer and employed SILAR method to incorporate the AgNPs into the device. The optical characteristics of the sensitizer, AgNPs and photoanode of the device were determined using UV-Vis spectrophotometer. The performance efficiency of the device was measured under AM1.5 at 100mW/cm^2 solar simulation. From the findings, using chlorine e_6 could potentially function as an efficient sensitizer for wide bandgap semiconductors like m-TiO_2 for visible light sensitisation. The incorporation of Ag NPs improved the light absorption in the visible region by the photoanode, and this enhancement is attributed to a peculiar characteristic of the Ag NPs surface plasmon resonance band which agrees well with the Mie theory for the surface plasmon peak of nanoparticles in UV-visible absorption spectra. The overall cell efficiency improvement could be explained by the quantum and surface phenomenon associated with the properties of Ag NPs; Ag NPs modify the interaction of the incoming light and the surface of the TiO_2 through their strong light absorption and scattering activity as a result of localised surface plasmon resonance (LSPR) which stem from a collective oscillation of the surface electrons that occurs when light interacts with a particle at its resonant frequency. Hence, the use of chlorine e6 in this study function efficiently as light harvester in the DSSCs and incorporation of AgNPs effectively enhanced the light harvesting capacity and as well improved the efficiency of the DSSCs.

REFERENCES

Allen, M. R., Frame, D. F., Huntingford, C., Jones, C. D., Lowe, J. A., Meinshausen, M. and Meinshausen, N. (2009). Warming caused by cumulative carbon emissions towards the trillionth tonne. *Nature,* **458**: 1163-1166.

Amao, Y., and Komori, T. (2004). Bio-photovoltaic conversion device using chlorine-e6 derivedfrom chlorophyll from Spirulina adsorbed on ananocrystalline TiO2 film electrode. *Biosensors and Bioelectronics,* **19:** 843–847.

Amiri, M., Nouhi, S. and Azizian-Kalandaragh, Y. (2015). Facile synthesis of silver nanostructures by using various depositionpotential and time: A nonenzymetic sensor for hydrogen peroxide. *Materials Chemistry and Physics,* **155**: 129-135.

Blaabjerg, F. and Ionel, D. M. (2015). Renewable Energy Devices and Systems – State-of the-Art Technology, Research and Development,Challenges and Future Trends. *Electric Power Components and Systems*, **43**(12): 1319 - 1328.

Chen, F. and Johnston, R. L. (2009). Plasmonic properties of silver nanoparticles on two substrates. *Plasmonics,* **4**: 147-152.

Chen, Q., Zhou, H., Hong, Z., Luo, S., Duan, H.-S., Wang, H.-H., . . . Yang, Y. (2014). Planar Heterojunction Perovskite Solar Cells via Vapor-Assisted Solution Process. *Journal of the American Chemical Society,* **136**:622–625.

Chien, T., Pavaskar, P., Hung, W. H., Cronin, S., Chiu, S. -H. and Lai, S. -N. (2015). Study of the Plasmon Energy Transfer Processes inDye Sensitized Solar Cells. *Journal of Nanomaterials,* **139243**: 1 - 6.

Dar, M. H., Ramos, F. J., Xue, Z., Liu, B., Ahmad, S., Shivashankar, S. A., . . . Grätzel, M. (2014). Photoanode Based on (001)-Oriented Anatase Nanoplatelets for Organic–Inorganic Lead Iodide Perovskite Solar Cell. *Chemistry of Materials,* **26**(16): 4675–4678.

Duran, E., Andujar, J. M., Enrique, J. M. and Perez-Oria, J. M. (2012). Determination of PV Generator I-V/P-V Characteristic Curves Using a DC-DC Converter Controlled by a Virtual Instrument. *International Journal of Photoenergy,* **843185**: 1-13.

Gharibshahi, L., Saion, E., Gharibshahi, E., Shaari, A. H. and Matori, K. A. (2017). Structural and Optical Properties of Ag Nanoparticles Synthesized by Thermal Treatment Method. *Materials,* **10**(402), 1 - 13.

Hara, K., Sato, T., Katoh, R., Furube, A., Ohga, Y., Shinpo, A., . . . Arakaw, H. (2003). Molecular design of coumarin dyes for efficient dye-sensitized solar cells. *The Journal ofPhysical Chemistry B,* **109**(2): 597–606.

Huang, C. -P. and Zhu, Y. -Y. (2007). Plasmonics:Manipulating Light at the Subwavelength Scale. *Active and Passive Electronic Components,* **30946**: 1-13.

Isah, K. U., Jolayemi, B. J., Ahmadu, U., Kimpa, M. I. and Alu, N. (2016). Plasmonic effect of silver nanoparticles intercalatedinto mesoporous betalain-sensitized-TiO2 film electrodeson photovoltaic performance of dye-sensitized solar cells. *Materials for Renewable and Sustainable Energy,* **5**(10): 1-10.

Jing, H., Zhang, L. and Wang, H. (2013). Geometrically Tunable Optical Properties of Metal Nanoparticles. In C. S. Kumar, *UV-VIS and Photoluminescence Spectroscopy for Nanomaterials Characterization* (pp. 1-74). Berlin: Springer.

Jolayemi, J. B. (2016). *Facile synthesis of plasmonic silver nanoparticles and application in dye sensitised solar cells.* Minna: Department of Physics, Federal University of Technology, Minna.

Khan, M. A., Kumar, S., Ahamed, M., Alrokayan, S. A. and AlSalhi, M. S. (2011). Structural and thermal studies of silvernanoparticles and electrical transport study oftheir thin films. *Nanoscale Research Letters,* **6**(434): 1-8.

Kim, H.-S., Lee, J.-W., Yantara, N., Boix, P. P., Kulkarni, S. A., Mhaisalkar, S., . . . Park, N.-G. (2013). High Efficiency Solid-State Sensitized Solar Cell-Based on Submicrometer Rutile TiO2 Nanorod and CH3NH3PbI3 Perovskite Sensitizer. *Nano Letters,* **13**(6): 2412–2417.

Lightbourne, S. K., Gobeze, H. B., Subbaiyan, N. K. and D'Souza, F. (2015). Chlorin e6 sensitized photovoltaiccells: effect of co-adsorbents on cell performance, charge transfer resistance, and charge recombination dynamics. *Journal of Photonics for Energy,* **5**: 053089-1 - 053089-11.

Mafune, F., Kohno, J., Takeda, Y., Kondow, T. and Sawabe, H. (2000). Structure and stability of silver nanoparticles in aqueous solutionproduced by laser ablation. *Journal of Physical Chemistry B,* **104**(35): 8333–8337.

Nanocomposix. (2017). *Silver Nanoparticles: Optical Properties*. Retrieved from nano Composix: https://nanocomposix.com/pages/silver-nanoparticles-optical-properties

O'Regan, B. and Gratzel, M. (1991). A low-cost, high-efficiency solar cell based on dye sensitized colloidal TiO2 films. *Nature,* **353**:737—740.

Petit, C., Lixon, P. and Pileni, M. (1993). In situ synthesis of silver nanoclusterinAOT reverse micelles. *Journal of Physical Chemistry,* **97**(49): 12974–12983.

Power, A., Cassidy, J. and Betts, T. (2011). Non aggregated colloidal silver nanoparticle for surface enhanced raman spectroscopy. *The Analyst,* **136**:2794-2801.

REN21. (2017). *Renewables 2017 Global Status Report.* Paris, France: Renewable Energy Policy Network for the 21st Century. Retrieved from http://www.ren21.net/status-of-renewables/global-status-report/

Thamilselvi, V. and Radha, K. V. (2017). A Review On The Diverse Application Of Silver Nanoparticle. *IOSR Journal Of Pharmacy,* **7**(1): 21-27.

Thiwawong, T., Onlaor, K. and Tunhoo, B. (2013). A Humidity Sensor Based on Silver Nanoparticles Thin Film Prepared by Electrostatic Spray Deposition Process. *Advances in Materials Science and Engineering,* **640428**: 1 - 7.

Wang, X. -F. and Kitao, O. (2012). Natural Chlorophyll-Related Porphyrins and Chlorins forDye-Sensitized Solar Cells. *Molecules,* **17**: 4484-4497.

Wang, X. -F., Tamiaki, H., Kitao, O., Ikeuchi, T. and Sasaki, S. (2013). Molecular engineering on a chlorophyll derivative, chlorin e6,for significantly improved power conversion efficiency indye-sensitized solar cells. *Journal of Power Sources,* **242**: 860-864.

Xu, Q., Liu, F., Liu, Y., Cui, K., Feng, X. Z. and Huang, Y. (2013). Broadband light absorption enhancement in dye-sensitized solarcells with Au–Ag alloy popcorn nanoparticles. *Scientific Reports,* **3**: 1-7.

Xu, Q., Liu, F., Liu, Y., Meng, W., Cui, K., Feng, X., . . . Huang, H. (2014). Aluminum plasmonic nanoparticles enhanced dye sensitized solar cells. *Optical Express A,* **301**(22): 1-10.

Zong, R., Wang, X., Shi, S. and Zhu, Y. (2014). Kinetically controlled seed-mediated growthof narrow dispersed silver nanoparticles up to120 nm: secondary nucleation, size focusing,and Ostwald ripening. *Physical Chemistry Chemical Physics,* **16**: 4236--4241.